An experimental study of the flowing granular layer in a rotating tumbler

Nitin Jain
Department of Chemical Engineering, Northwestern University, Evanston, Illinois 60208

J. M. Ottino
Department of Chemical Engineering and Department of Mechanical Engineering, Northwestern University, Evanston, Illinois 60208

R. M. Lueptow
Department of Mechanical Engineering, Northwestern University, Evanston, Illinois 60208

(Received 22 February 2001; accepted 1 November 2001)

Granular flow in a rotating tumbler is of theoretical and industrial significance. However, in spite of its relative simplicity, little is known about the dynamics of the top flowing layer. Here we present an experimental study of the velocity field within the fluidized layer of monodisperse particles in a quasi-2D (two-dimensional) rotating tumbler in the rolling flow regime using particle tracking velocimetry. The granular flow is illuminated by a laser flash and recorded using a charge coupled device camera. Image processing is used to remove the experimental noise and to achieve *sub-pixel* accuracy in calculating the particle displacements. The ensemble-averaged streamwise and transverse velocity profiles are calculated based on the particle displacements for three angular velocities and three bead sizes. The normalized streamwise velocity profile is linear throughout the fluidized layer, but becomes logarithmic as it enters the ''fixed'' bed where slow particle rearrangements dominate. The rms velocities appear to be exponentially related to the depth in the layer. Nondimensionalizing the number density in the fluidized layer with a geometric factor based on the square packing results in collapse of the data over a range of bead sizes and angular velocities. © *2002 American Institute of Physics.* [DOI: 10.1063/1.1431244]

I. INTRODUCTION

An understanding of granular flows, in particular tumbling, is of practical importance given numerous applications in the pharmaceutical, cement, polymer, agrochemical, and metallurgical industries. Horizontal cylindrical rotating tumblers partially filled with granular material are used industrially for mixing, calcination, and coating operations. Depending on the speed of rotation, different flow regimes occur—avalanching, rolling or cascading, cataracting, and centrifuging.[1–3] This paper focuses exclusively on the rolling regime. The bulk of the material in the fixed bed rotates as a solid body (except for slow particle rearrangements)[4] until it reaches its dynamic angle of repose, and the flowing material is confined to the thin layer rolling down the free surface. The flow at the free surface is steady, and the free surface is nearly flat. The shape of the flowing layer is lenticular and in the case of our experiments is 5–10 particles thick, depending on the speed of rotation.

Unlike liquid mixing,[5] a complete understanding of granular mixing is hindered by the absence of an accepted set of governing equations. Attempts have been made to model mixing and segregation of granular material from a continuum viewpoint.[3,6,7] Models for the advection of the particles often depend on the velocity profile and the particle number density variation in the flowing granular medium. For example, in a continuum mechanics model for transverse flow, both a linear velocity profile and a Bagnold velocity profile as well a constant number density in the flowing layer and the bed have been used.[6]

The most detailed experimental study measuring the velocity profile in the fluidized layer of a rotating tumbler is the work by Nakagawa *et al.* using magnetic resonance imaging (MRI).[8] These investigations found that: (i) The velocity profile is approximately linear except near the interface between the layer and the bed; (ii) the velocity varies along the length of the layer with a maximum near the center of the layer; and (iii) the number density decreases across the flowing layer from the bed to the free surface. However, this work was qualitative in nature and was focused on the capability of MRI for measuring granular flows. Furthermore, the parameter space that was studied was limited. Only the angular velocity of the system was varied, while other parameters such as bead size and bead density were held constant. Ristow performed a molecular dynamics simulation of the flowing layer and obtained results that were qualitatively similar to those of Nakagawa.[9] But once again, only the angular velocity was varied.

Our objectives in this paper are twofold. First, we describe a method to apply particle tracking velocimetry (PTV) to the measurement of the velocity and number density profiles in a 2D granular flow. Several techniques in addition to MRI are suitable for opaque, three-dimensional (3D) granular flows including positron emission particle tracking,[10] x-ray imaging,[11] radioactive tracers,[12] diffusing wave spectroscopy,[13] fiber-optic probes,[14] and layering of granules of different colors.[15]

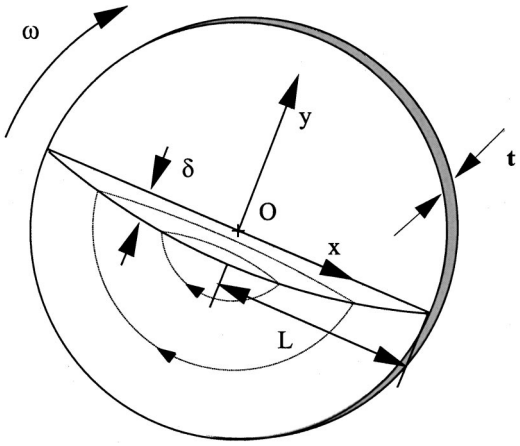

FIG. 1. The rotating tumbler geometry with the coordinate system and the system parameters. Curves indicate the path of particles.

Optical velocimetry techniques such as particle image velocimetry (PIV) are an effective means to measure the velocity in 2D granular flows with high temporal and spatial resolution.[16–19] PIV, which is commonly used for measuring fluid flows, applies cross-correlation techniques to images of granular particles in a visible plane of the flow to measure the statistically averaged displacement and velocity of particles in a small region of the image. PTV, which is based on the measurement of individual particle displacements, allows the acquisition and analysis of an enormous amount of data with high spatial resolution. Unlike PIV, PTV is insensitive to steep velocity gradients. This is especially important for the thin fluidized layer in a rotating tumbler. Of course, the opacity of the particles limits PTV to quasi-two dimensional flows observed through a clear window. This quasi-2D geometry can result in a small tangential friction force even with smooth endwalls, but in general this wall friction is small relative to the interparticle friction and collisional forces.[20] Finally, an understanding of two-dimensional flows is often central to the understanding of three-dimensional flows,[21–26] and the PTV technique presented here can easily be extended to many other quasi-2D granular flows.

Our second objective is to thoroughly investigate the character of the flowing layer of a granular media in a rotating tumbler to provide a better understanding of this fundamental granular flow. We include profiles of the streamwise velocity, transverse velocity, granular temperature, and number density for variations in the size and density of the granular particles as well as the rotational speed of the 2D tumbler. We scale the velocity profile and number density profile based on physical arguments. Such scaling results are of direct utility in engineering design for scale-up of large systems based on experimental results from small systems.[27] The relationships presented here appear to work reasonably well for the parameter space studied.

II. EXPERIMENTAL PROCEDURE

The 2D circular tumbler is shown schematically in Fig. 1. The flowing layer has a lens-like shape. The predominant velocity is in the x direction. Since the flow region is a function of x, it follows that the streamwise velocity is $u=u(x,y)$. By continuity, there exists a transverse velocity $v=v(x,y)$. The actual system is 28 cm in diameter $(2L)$. The back surface of the tumbler is an aluminum plate anodized black to minimize the optical noise effects in the PIV/PTV images. The front face-plate is clear acrylic to permit optical access. The axial thickness of the tumble (t) is varied from 3.2 to 9.5 mm by using various thickness spacers, acrylic sheets with a 28 cm hole, between the front and the back plates. The tumbler diameter is more than an order of magnitude larger than the thickness of the tumbler to assure a nearly two-dimensional flow of the granular material. A computer controlled stepper motor rotates the tumbler at speeds (ω) between 0.052 and 0.168 rad/s, corresponding to an order of magnitude change in the Froude number, $Fr=\omega^2 L/g$, from 0.39×10^{-4} to 4.0×10^{-4}.

Spherical glass beads with diameters (d) of 1 mm (0.99 ± 0.04 mm), 2 mm (2.05 ± 0.08 mm), and 3 mm (3.00 ± 0.008 mm) (Quackenbush Co.) are used for the experiments. The dimensionless thickness of the rotating tumbler is set at $t/d=3.2$ to ensure the same effective two-dimensionality for all bead sizes and to maintain similarity with respect to this parameter. The filling fraction for all experiments is 50%.

The key results of this work are the streamwise (x-component) velocity (u) and transverse (y-component) velocity (v) along with the number of particles (N) as functions of the transverse coordinate (y). Most measurements are made near the center of the rotating tumbler $(x=0)$ where the thickness of the flowing layer (δ) is greatest. A small number of measurements are made both upstream and downstream of the center.

The clear side of the tumbler is illuminated by dual-YAG laser system (532 nm) in a back-scatter mode. The cylindrical beam passes through a diffuser plate to generate a broad flash of light. The light reflected back from the layer of particles adjacent to the clear sidewall of the tumbler is recorded by a standard PIV system having a charge coupled device (CCD) camera with a resolution of 1016×1000 pixels. The PIV system synchronizes the camera, laser flashes, and frame grabber to obtain pair of images separated by a small time delay ($\sim10^{-3}$ s). Pairs of images are obtained at a frequency of 15 Hz. The camera's field of view is set to capture a region about 3 cm square, corresponding to 10–30 particle diameters. Typically, 99 image pairs are obtained over several seconds of steady-state operation.

The procedure to calculate the velocity vectors requires four steps: (i) Image processing to improve the image quality; (ii) locating the centers of particles; (iii) PIV calculation to guide PTV calculations; and (iv) PTV calculations to obtain final velocity vectors. Image processing is necessary to remove non-ideality introduced by the imaging and illumination system. A sample of the raw image of the flowing layer is shown in Fig. 2(a). The particles are approximately 30–50 pixels in size, depending on the magnification. The black background minimizes noise making the image threshold more effective. Upon illumination, the beads have a small, bright spot near their center that is about 10 pixels in diameter. The bright spot is tracked and the remaining portion of

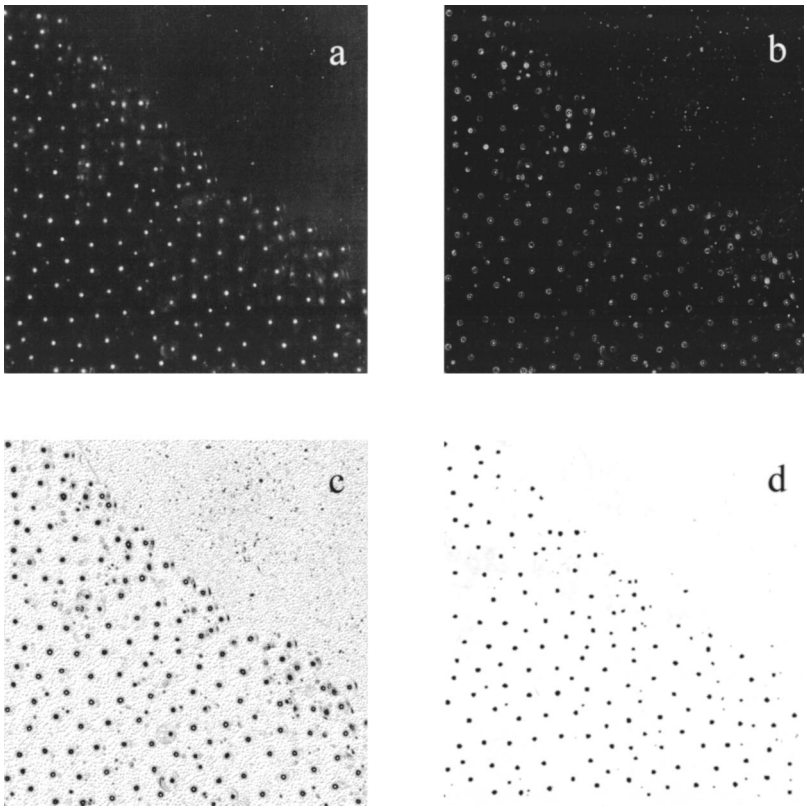

FIG. 2. Image processing steps used to minimize the background noise: (a) Raw image; (b) after edge detection; (c) after dithering; (d) final processed image after erosion.

the bead in the image is eliminated by thresholding. However, reflections and scratches on the acrylic window interfere with the image clarity and are not easily removed by simple thresholding making further image processing necessary. The first step is edge detection resulting in large size dots corresponding to the bright spot on the beads and small spots corresponding to noise as shown in Fig. 2(b). Converting the intensity to ''on'' or ''off'' for each pixel (dithering) provides a negative image like that shown in Fig. 2(c). The dithered image is eroded to remove the small spots related to noise resulting in the image shown in Fig. 2(d). After erosion, the top right portion of the image indicates that the image is nearly free of noise.

Sub-pixel accuracy in finding the location of individual particles is achieved by masking the original image [Fig. 2(a)] with the processed image [Fig. 2(d)]. The black regions in the processed image pick up the intensity from the original image while the white regions are set to zero. A Gaussian surface is then fitted to the intensity distribution for each particle to identify the center of the particle with subpixel resolution.

Although we have successfully applied PIV to granular flow,[18] the flow considered here presents unique difficulties and is a more stringent test of the technique. The fluidized layer in a rotating tumbler is only 5–10 particles thick and has a very steep velocity gradient. Consequently, having an adequate number of particles in the PIV interrogation region requires it to be as large as the thickness of the layer resulting in inadequate spatial resolution. The problem can be solved by calculating the displacement of individual particles using PTV guided by crude estimates of the velocity field obtained with PIV as suggested by Cowen and Monismith.[28] Based upon the particle location in the first image and the PIV approximation of the velocity field, the position of the particle in the second image of the pair is predicted. To improve the prediction, a cross-correlation between the particle location in the first image and the predicted position in the second image is calculated for a square region 7 pixels on a side. A Gaussian surface is fitted to the cross-correlation peak to determine the spatial shift corresponding to maximum correlation value to sub-pixel resolution.[28] A particle in the second image is taken as the pairing particle only if it is the only particle present within the specified vicinity of the estimated position.

Figure 3 is a sample of the displacement vectors generated from a pair of images for the region shown approximately in figure's inset. The velocity vectors are calculated from the displacement vectors using the time delay between the two images of an image pair. Since the velocity is much higher at the surface of the flowing layer than at the interface between the layer and the bed, three different time delays between images are used for each experimental condition to provide adequate resolution of the displacement through the depth of the flowing layer. The results are overlaid to obtain optimal resolution of the velocity. One problem with interpreting the data from measurements like those in Fig. 3 is determining the location of the surface of the flowing layer. To do this, displacement vectors from 99 image pairs are overlaid to create a plot similar to Fig. 3 except with a much higher density of vectors. Then a line parallel to the flow is positioned as close as possible to the vectors so that all but

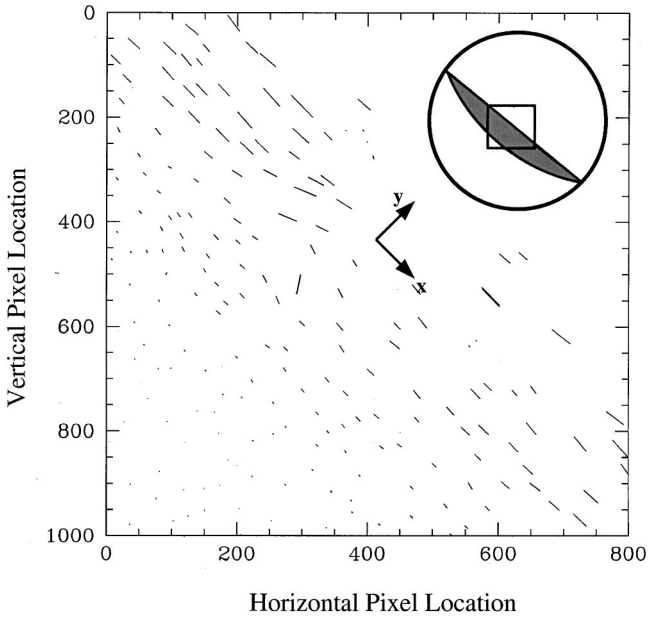

FIG. 3. Sample displacement vectors generated from a pair of images using PTV. The square region in the inset shows the approximate position of the image region, although the size of the image region is not to scale.

obviously extraneous vectors are enclosed. This line is set to $y=0$.

Images of the bead positions like that shown in Fig. 2(d) are also used to determine the bead number density profile in the flowing layer. A rectangular window of length ~2 cm (800 pixels) perpendicular to the flowing surface and width ~1 cm (400 pixels) along the flowing surface is used for the number density calculation. (The narrow dimension parallel to the flowing surface is necessary to avoid double-counting particles consecutive images.) This window is divided into a number of bins perpendicular to the flowing surface, and the number of particles present in each bin is summed.

III. RESULTS

To obtain the velocity profile in the flowing layer, the velocities of the particles in a narrow strip about three particles wide in the streamwise x-direction and extending into the fixed bed in the transverse y direction at the center of the tumbler ($x=0$) are collected from all 297 image pairs (99 image pairs at each of three delays between images). The delay between image pairs is long enough so that the same particles do not appear in the narrow strip for consecutive image pairs except very near the fixed bed. The dimensionless streamwise (u) and transverse (v) velocity profiles for the particles are plotted in Fig. 4 for 3 mm spherical glass beads tumbled at 0.168 rad/s. The velocity profile is plotted in the traditional boundary layer format with the velocity plotted along the horizontal axis as a function of the distance from the top of the flowing layer plotted along the vertical axis. In this figure, the radius of the tumbler (L) and angular velocity (ω) are used for nondimensionalization. The large number of particle velocity measurements provides statistically meaningful information about the flow dynamics. The solid curves represent the average velocity profile and the

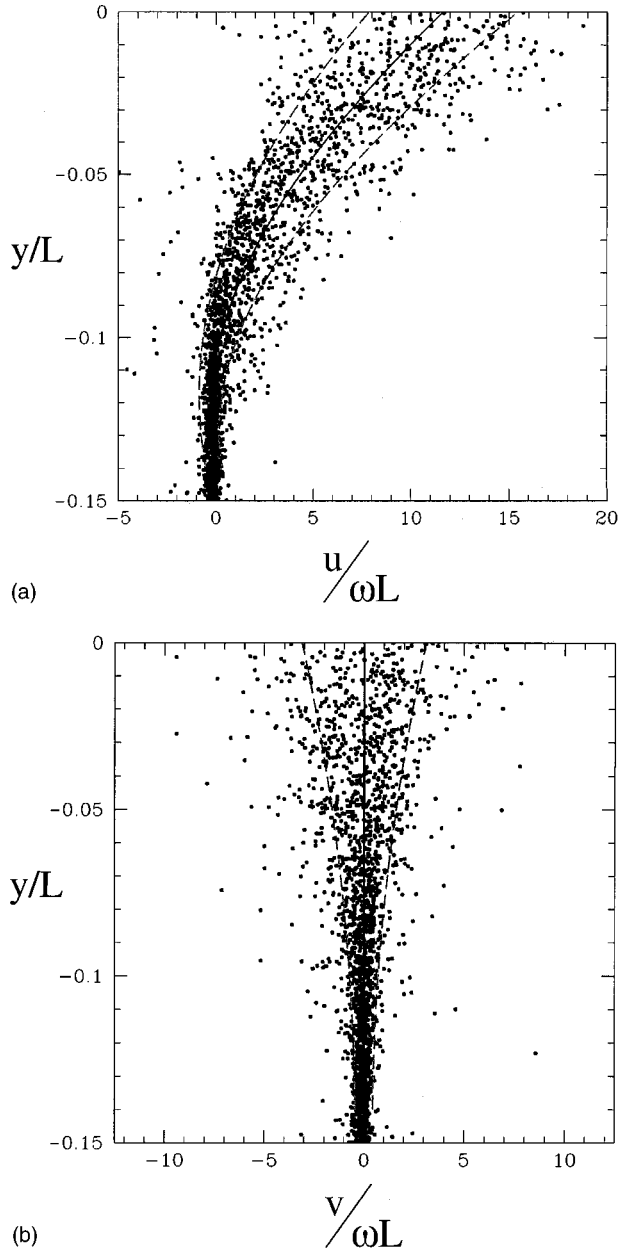

FIG. 4. Scatter plot of streamwise (u) and transverse (v) velocities for 3 mm beads rotated at 0.168 rad/s as a function of depth (y) at $x=0$. The solid curve is a third-order polynomial fit through the data. The dashed curves on either side of the solid curve correspond to one standard deviation.

dashed curves represent one standard deviation from the average profile. Except for the mean transverse velocity profile, which is a line at $v=0$, the curves are based on a third-order polynomial fit through the mean and standard deviation calculated for each of 20 bins in the transverse direction. The scatter in the particle velocities increases near the flowing surface and decreases near the interface between the flowing layer and the fixed bed. The average transverse velocity component is negligible with an equal scatter on both sides of $v=0$. The standard deviation is only slightly larger for the streamwise velocity than for the transverse velocity.

Of key interest is a scaling law for the velocity profile. The simplest situation corresponds to a half-full cylinder with a thin flowing layer, $\delta/L \ll 1$, as is the case in these

experiments. Assume that the number density of particles in the flowing layer is similar to that in the fixed bed. Since the bed rotates essentially as a solid body, all of the materials pass through the flowing layer in half a revolution. Therefore, the volumetric flow rate in the layer per unit cylinder thickness calculated at the midpoint ($x=0$) is

$$Q_0=\frac{\pi L^2}{2}\frac{\omega}{\pi}=\frac{\omega L^2}{2}. \tag{1}$$

Thus, the average velocity in the flowing layer is

$$u_{\mathrm{av}}=\omega L^2/(2\delta_0), \tag{2}$$

where δ_0 is the thickness of the flowing layer at $x=0$. A more detailed analysis can be done by taking into account the finite thickness of the layer.[6] The error of the approximation is $(\delta_0/L)^2 \ll 1$. Based on Eq. (2), the velocity should scale with $\omega L^2/\delta$.

Using this scaling requires that δ be determined from the data. Considerable care is necessary in determining δ to avoid a bias due to assumptions about the shape of the velocity profile, which, for instance, could occur by fitting a polynomial to the velocity profile. Instead, the flowing layer is subdivided into 20 bins, so that the average streamwise velocity in the last bin (nearest the fixed bed) has a zero or slightly negative value, while all other bins are positive. The flowing layer thickness and other important parameters of the flow are summarized in Table I.

The average streamwise velocity is plotted using the above scaling for 3 mm beads at three different rotational speeds in Fig. 5(a). The scaling results in collapse of the data for 0.052 rad/s$\leqslant\omega\leqslant$0.168 rad/s. Figure 5(b) shows a similar collapse for three different bead sizes (1, 2, and 3 mm) tumbled at rotational speed of 0.052 rad/s.

The velocity profiles for three different bead sizes and three different rotational speeds (nine cases) are shown in Fig. 6(a). The universality in the scaled velocity profile breaks down. Two different, but qualitatively similar, streamwise velocity profiles result. One set of profiles results for small beads (1 and 2 mm) and high angular velocities (0.094 and 0.168 rad/s); the other set of profiles is for small beads (1 and 2 mm) at a low angular velocity (0.052 rad/s) and for large beads (3 mm). A possible reason for nonuniversality may have to do with the size dependence for transition between the rolling and cataracting regimes. For smaller beads at high angular velocities, the varying interchange rate between the fixed bed and the flowing layer results in the surface tending toward a slight *s*-shape.[29] For this reason the 3 mm beads collapse to a single profile for the different angular velocities while 1 and 2 mm beads fall onto one of two velocity profiles, depending on the angular velocity. Thus, the physics of the flow changes as the bead size and angular velocity change resulting in two different scaled velocity profiles, one for each of the two different flow regimes.

TABLE I. Granular flow parameters at $x=0$.

d (mm)	Material	Ω (rad/s)	δ_0 (mm)	$u_{\max}$ (m/s)
1	glass	0.052	8.4	0.187
1	glass	0.094	9.1	0.507
1	glass	0.168	9.8	0.709
2	glass	0.052	9.8	0.173
2	glass	0.094	11.9	0.335
2	glass	0.168	13.3	0.548
3	glass	0.052	12.6	0.118
3	glass	0.094	14.0	0.216
3	glass	0.168	15.4	0.260
2	steel	0.094	16.8	0.263
2	steel	0.168	18.2	0.462

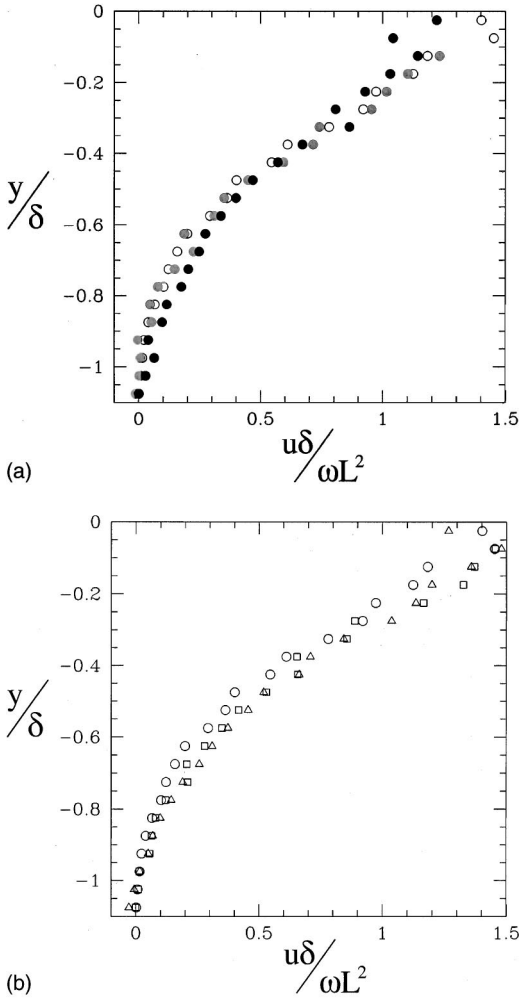

FIG. 5. Scaled streamwise velocity profile at $x=0$. (a) 3 mm beads at 0.052, 0.094, and 0.168 rad/s. (b) 1, 2, and 3 mm beads at 0.052 rad/s. Symbols: ▲, 1 mm beads; ■, 2 mm beads; ●, 3 mm beads. Symbol fill: open, 0.052 rad/s; gray, 0.094 rad/s; black, 0.168 rad/s.

Another ''scaling'' is shown in Fig. 6(b), where the streamwise velocity profile is normalized using the maximum velocity at the top of the flowing layer, $u_{\max}$. Using $u_{\max}$ to nondimensionalize the velocity is not truly a scaling based on independent parameters of the system, but it is useful to show the similarity of the velocity profiles much like the measured boundary layer thickness or friction velocity are used in the analysis of turbulent boundary layer velocity profiles. This figure indicates a somewhat better, though not perfect, collapse of the nine experimental cases than Fig. 6(a), and this collapse seems to be independent of small changes in the physics of flow. More importantly, the

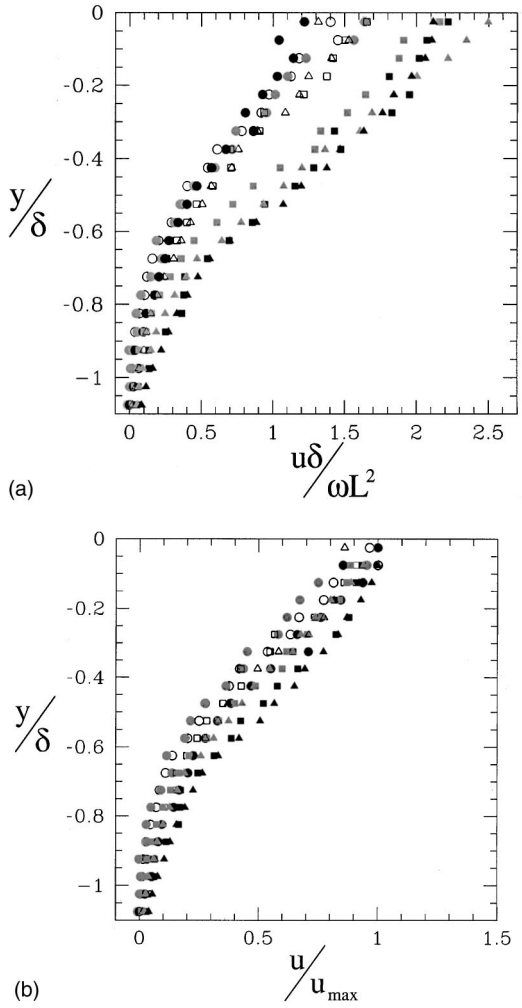

FIG. 6. Streamwise velocity profile at $x=0$ for nine cases. (a) Scaling of velocity based on mass balance; (b) velocity normalized by the velocity at the surface of the flowing layer, u_{max}. Symbols: ▲, 1 mm beads; ■, 2 mm beads, ●, 3 mm beads. Symbol fill: open, 0.052 rad/s; gray, 0.094 rad/s; black, 0.168 rad/s.

similarity in the velocity profiles is evident in Fig. 6(b). The velocity profile is nearly linear from the surface of the flowing layer well into the layer, smoothly approaching zero velocity near the fixed bed. These results are similar to those for the flowing layer of a 3D tumbler at a lower fill (8%–15%) measured using an invasive, fiber optic probe.[14]

It is helpful to plot the streamwise velocity using semilog and log–log coordinates in an attempt to characterize the velocity profiles. Figure 7 shows the same data in Fig. 6(b), except plotted using various logarithmic coordinates. Using a logarithmic scale for the transverse coordinate in Fig. 7(a), suggests that $u/u_{max} \sim \ln(-y/\delta)$ in the lower part of the layer near the fixed bed. But the logarithmic dependence of velocity on transverse position breaks down in the upper half of the flowing layer ($\ln(-y/\delta) < -0.7$). The other alternative for a semilog plot shown in Fig. 7(b) does not collapse the data. Not surprisingly, plotting the velocity profile using log–log coordinates collapses the data fairly well, as indicated in Fig. 7(c). But it fails to suggest a power law relation. Consequently, Fig. 6(b) showing a velocity profile that is nearly

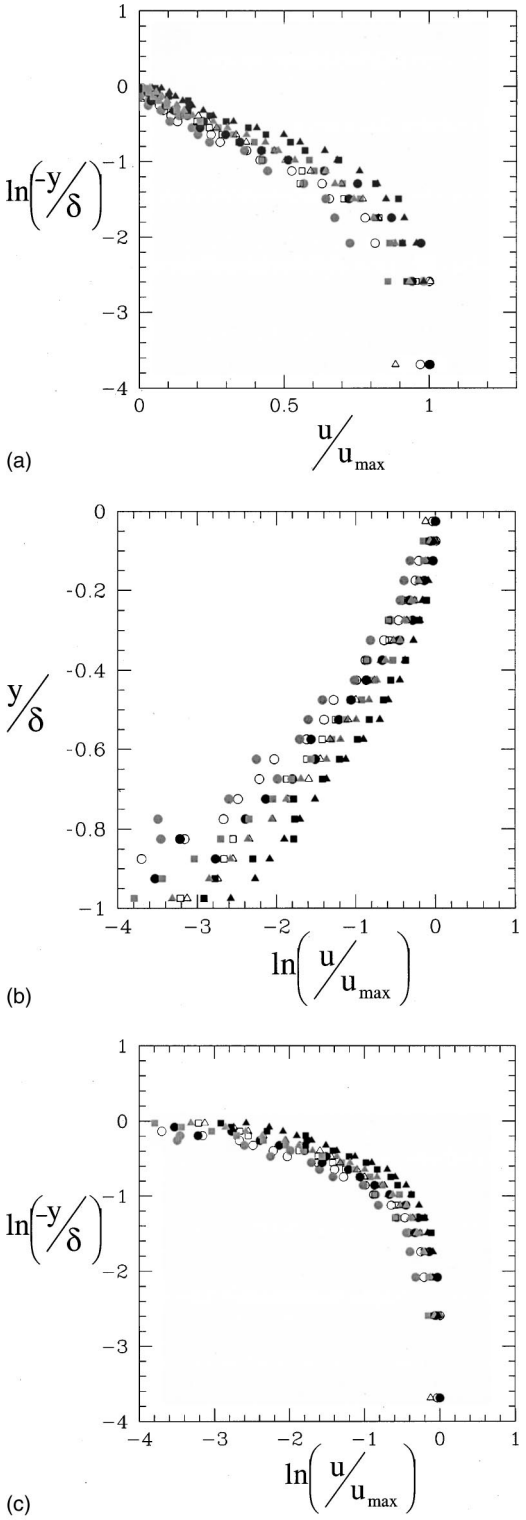

FIG. 7. Replotting the streamwise velocity profile at $x=0$ in various forms. Symbols: ▲, 1 mm beads; ■, 2 mm beads; ●, 3 mm beads. Symbol fill: open 0.052 rad/s; gray, 0.094 rad/s; black, 0.168 rad/s.

linear from the surface of the flowing layer and Fig. 7(a) showing the velocity profile logarithmically approaching zero velocity near the fixed bed seems to best describe the streamwise velocity profile.

To test the effects of particle density on the velocity field, experiments are also performed for steel beads with a

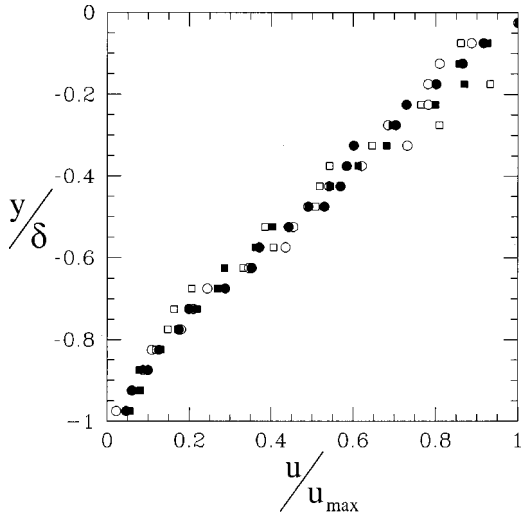

FIG. 8. Streamwise velocity profile at $x=0$ for 2 mm glass and steel beads. Symbols: ■, glass beads; ●, steel beads. Symbol fill: open, 0.094 rad/s; black, 0.168 rad/s.

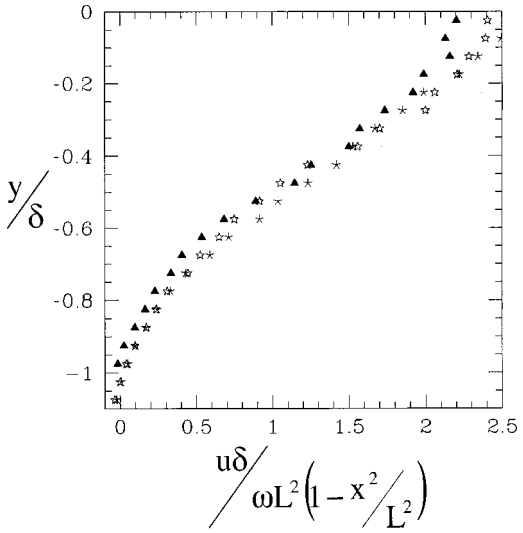

FIG. 9. Scaling of the streamwise velocity profile with change in the streamwise location (x) along the layer for 1 mm beads at 0.168 rad/s. Symbols: ▲ $x=0$; ☆ $x/l=-0.57$; skeletal star, $x/L=0.70$.

diameter of 2 mm and a density of 7.5 g/cm^3 (compared to a density of 2.5 g/cm^3 for glass beads). Like the glass beads, the steel beads are also coated black for optimal image processing. Velocity measurements are made at $x=0$ for $\omega=0.094$ rad/s and $\omega=0.168$ rad/s. A comparison of the velocity profiles for steel and glass beads are shown in Fig. 8. The velocity profiles for the steel and glass beads overlap suggesting that the streamwise velocity profile and its scaling may be independent of the bead density. This result is consistent with the similarity in the shape of the flowing layer cross-section for identical Froude number and bead size, independent of particle density.[29] However, the apparent similarity in the velocity profile still needs to be examined over a wider range of sizes, densities, and rotational speeds.

The scaling arguments presented to this point are limited to the center of the flowing layer. The previous mass balance argument can be generalized to scale the velocity profiles measured at any streamwise location along the layer. For a layer of thickness $\delta(x)$ at position x, the distance along a radial line from the flowing layer-bed interface to the wall of the tumbler is $L-\sqrt{x^2+\delta^2}$. Consequently, the distance from the center of rotation to the midpoint of the fixed bed along this line is $(L+\sqrt{x^2+\delta^2})/2$. Assume the density in the flowing layer is about the same as that in the bed. Then mass balance for the flowing layer and the fixed bed results in

$$u_{\mathrm{av}}\delta=\left[\left(\frac{L+\sqrt{x^2+\delta^2}}{2}\right)\omega\right](L-\sqrt{x^2+\delta^2}), \tag{3}$$

which is identically zero at $x=\pm L$, since $\delta(\pm L)=0$. This equation can be rewritten as

$$u_{\mathrm{av}}=\frac{\omega L^2}{2\delta}[1-(x/L)^2-(\delta/L)^2]. \tag{4}$$

For $\delta_0/L\ll 1$, $u_{\mathrm{av}}\propto(\omega L^2/\delta)[1-(x^2/L^2)]$, similar to previous forms,[2] suggesting that the velocity scales as $u\delta/[\omega L^2(1-(x^2/L^2))]$. The scaling relation for the center of the layer $(x=0)$ is therefore a special case of this general scaling.

Experiments are performed using 1 mm beads at three locations: $x/L=-0.57$, $x/L=0$, and $x/L=0.70$. The streamwise velocity profiles at these three positions along the layer collapse using the above scaling as shown in Fig. 9. The collapse is remarkable given that the dimensional velocities differ by a factor of 2.

The transverse velocity also depends on the streamwise position. Figures 10(a) and 10(b) show the transverse velocity profile, v, at the upstream and downstream positions, respectively, based on 10 bins across the flowing layer. The velocity in these plots is scaled by the angular velocity and the radius of the tumbler while the transverse coordinate is scaled by the thickness of the flowing layer. The curve is a third-order polynomial fit to the data. At the upstream position, a net positive transverse velocity indicates particles moving upward in the layer, while the net negative transverse velocity at the downstream position indicates particles moving toward the bed. The transverse velocity is a maximum at the interface between the layer and the bed. A simple argument can lead to an expression for the transverse velocity at the interface between the bed and the flowing layer, v_{int}. To the extent that the bed is in solid body rotation, the inflows and outflows to the layer are largely kinematically defined, although the walls undoubtedly play a role. However, it is noncritical. An order of magnitude analysis shows that the wall effects may be relatively small.[20] In addition, Orpe and Khakhar[29] in a series of exhaustive experiments, considered a range of cylinder lengths and particle diameters as well as Froude numbers. Their results showed that the flow is relatively unaffected by the sidewalls for small values of d/L. For $x\gg\delta$, the transverse velocity of particles in the fixed bed at the interface is essentially the same as the azimuthal velocity due to rotation of fixed bed (v_θ) so that $v_{\mathrm{int}}\approx v_\theta|_{\mathrm{interface}}\sim -x\omega$. Therefore, the transverse velocity at the interface between the flowing layer and the fixed bed is $v_{\mathrm{int}}/\omega L\approx -x/L$. The transverse velocity at the interface indicated in Fig. 10 is very close to this prediction. At x/L

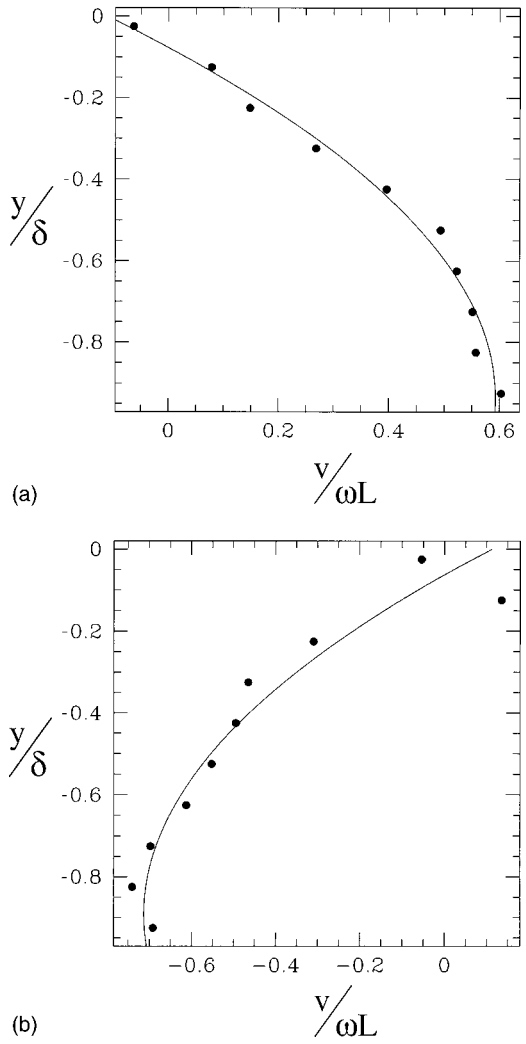

FIG. 10. Transverse velocity profile for 1 mm beads at 0.168 rad/s at two different locations: (a) Upstream at $x/L=-0.57$; (b) downstream at $x/L=0.70$.

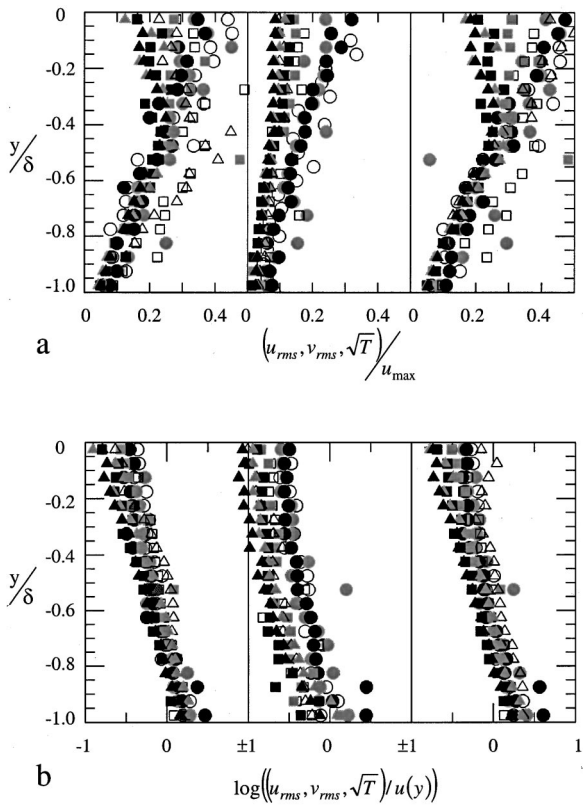

FIG. 11. Velocity fluctuations at $x=0$. (a) Profiles of the rms velocity fluctuations normalized by the maximum streamwise velocity, u_{max}. (b) Profiles of the rms velocity normalized by the local mean streamwise velocity, $u(y)$. Symbols: ▲, 1 mm beads; ■, 2 mm beads; ●, 3 mm beads. Symbol fill: open, 0.052 rad/s; gray, 0.094 rad/s; black, 0.168 rad/s.

$=-0.57$, the transverse velocity at the interface is $v_{int}/\omega L \approx 0.6$, and at $x/L=0.70$, the transverse velocity is $v_{int}/\omega L \approx -0.7$. It is also useful to compare the transverse velocity to the streamwise velocity at that streamwise location. At $x/L=-0.57$, $v_{int}/u_{max}=0.029$ and at $x/L=0.70$, $v_{int}/u_{max}=-0.037$. Even though the transverse velocity is only a small fraction of the surface velocity, it contributes significantly to transport processes and mixing within the layer.[7]

The instantaneous velocity of a granular particle can be expressed as the sum of the mean velocity and velocity fluctuation. To calculate the root-mean-square (rms) fluctuations in the streamwise direction (u_{rms}) and the transverse direction (v_{rms}), the transverse coordinate is once again divided into 20 bins and the average velocity and standard deviation for each of the bins is calculated for each velocity component for all data sets obtained at particular conditions. The time between images of an image pair ($\sim 10^{-3}$ s) is less than an estimate for the time scale for particle collisions ($d/u \sim 10^{-2}$ s, except for the 1 mm beads at the higher rotation rates), so it is unlikely that multiple particle collisions occur during the interval between images. In addition to calculating u_{rms} and v_{rms}, the granular temperature, which is a measure of the overall randomness, is calculated according to[30,31]

$$T=\langle \mathbf{u}^2\rangle-\langle \mathbf{u}\rangle^2=u_{rms}^2+v_{rms}^2, \tag{5}$$

where $\mathbf{u}=(u,v)$ is the velocity vector, and the angled brackets indicate a time average. The rms velocities and temperature profiles are presented in two different ways. In Fig. 11(a), the fluctuations are normalized by the streamwise velocity at the surface of the flowing layer, u_{max}, to show the relative magnitude of the velocity fluctuations throughout the layer. Clearly, the magnitude of the velocity fluctuations is greatest at the surface of the flowing layer and diminishes near the interface between the flowing layer and the fixed bed, as intuition would suggest. The streamwise fluctuations, u_{rms}, are somewhat larger than the transverse fluctuation, v_{rms}, but the difference is small. In both cases the fluctuations range from about 5% of the maximum streamwise velocity near the fixed bed to about 1/3 of the streamwise velocity near the surface. This is higher than the streamwise velocity fluctuations of 8% found using MRI or 2 to 4% found using an optical probe in 3D rotating tumblers at substantially different operating conditions.[14,32] The square root of the granular temperature can reach nearly half of the maximum velocity. The scatter in the data is greater near the surface of the flowing layer resulting in a poor collapse of the data over the range of particle diameters and angular velocities considered.

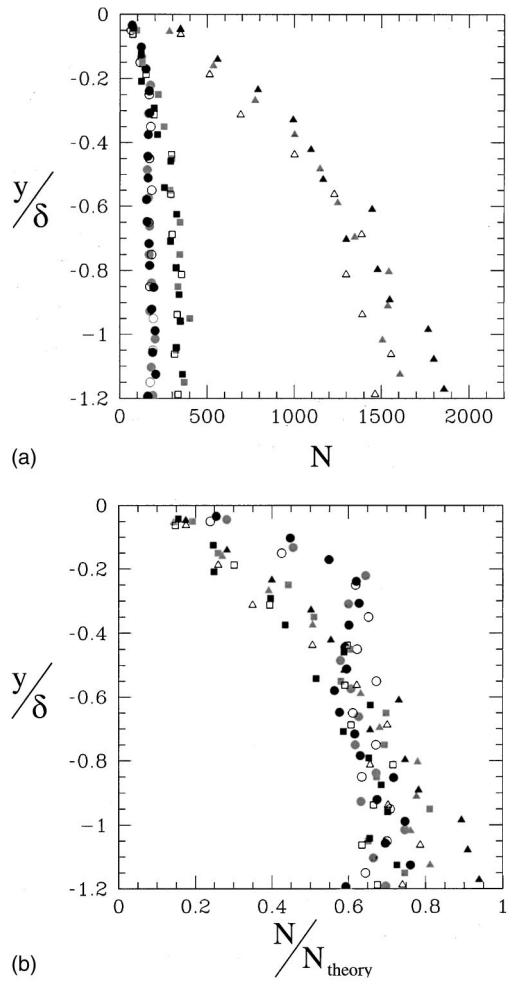

FIG. 12. (a) Total number of beads counted in each bin as a function of transverse position at $x=0$. (b) Normalized number density profiles. Symbols: ▲, 1 mm beads; ■, 2 mm beads; ●, 3 mm beads. Symbol fill: open, 0.052 rad/s; gray, 0.094 rad/s; black, 0.168 rad/s.

Nondimensionalizing the velocity fluctuations and temperature with the local streamwise velocity, $u(y)$, indicates the magnitude of the velocity fluctuations relative to the local velocity. Plotting the profile of the log of the value results in much better collapse of the data, as shown in Fig. 11(b). In addition, this nondimensionalization scheme provides different insight into the nature of the fluctuations. Although it is clear from Fig. 11(a) that the fluctuations are small deep in the flowing layer, Fig. 11(b) shows that these small fluctuations can be larger than the local average streamwise velocity near the fixed bed. The situation is reversed near the surface of the flowing layer where the velocity fluctuations are only a fraction of the local velocity. Furthermore, the fluctuations and temperature nondimensionalized by the local velocity are nearly exponential functions of depth in the layer. The physical reason for this is not immediately clear.

It is intuitively evident that the number density of particles in the fluidized flowing layer should be less than in the bed. Figure 12(a) shows the dependence of the profiles of the number of beads on the angular velocity and the bead size. The figure shows the number of beads counted in bins distributed in the transverse direction well into the fixed bed for 198 images. The curves assemble into three distinct profiles based on the bead diameter indicating that the number density of beads is independent of angular velocity. The number of beads is a minimum at the free surface and reaches a uniform maximum value in the nonflowing bed, in accordance with physical intuition. The difference in the total count of beads is imply due to the difference in the size of the beads compared to the fixed size of the interrogation region. The number of beads counted is highest for the small 1 mm beads and lowest for the large 3 mm beads.

The number of beads (N) visible in a two-dimensional region of fixed size is inversely related to d^2. A coarse inspection of Fig. 12(a) shows approximate agreement with this concept, $N_{\max}$ for 1 mm beads is around 1600 which is about 2^2 times the $N_{\max}$ for 2 mm beads. The number of beads of diameter d that could fit in a bin of area A if the flow is strictly two-dimensional is $N_{\text{theory}}=A/d^2$ for square packing. Although the granular flow is only quasi-two-dimensional, this theoretical value based on strictly two-dimensional packing is useful to scale the number of beads as N/N_{theory}. Figure 12(b) shows that this scaling leads to a clear trend in the bead number density profiles for different bead diameters and angular velocities compared to the unscaled results in Fig. 12(a). The scaled number density is near its maximum through the half of the layer nearest the fixed bed and drops off in the half of the layer nearest the free surface. The number of beads near the free surface is about 30% of the maximum number. We note that the region where the number density is large corresponds to the region for a logarithmic velocity profile [Fig. 7(a)], while the region where the number density is decreasing corresponds to the region having a linear velocity profile [Fig. 6(b)].

One may argue that the number density of particles could be inversely related to the velocity fluctuations of the particles, since a lower number density provides for the possibility of larger particle displacement, although a higher number density would lead to more collisions. To determine the nature of the relationship, the square root of the temperature is plotted against the normalized number density of beads in Fig. 13. While the data do not indicate a clear trend, there is a subtle relation between the temperature and the number density consistent with the idea of velocity fluctuations decreasing with increasing number density.

Looking at the data more closely, the relation seems to take a particular form for a given bead size. The temperature remains at a high level decreasing slowly with number density and then, at a certain number density, decreases sharply with increasing number density. This is readily evident for the case of 3 mm beads (circles). The temperature is about $\sqrt{T}/u_{\max}\approx 0.5$ for $N/N_{\text{theory}}\lesssim 0.6$, and then decreases quite quickly above this number density. Similar results occur for 1 mm beads and 2 mm beads except that the temperature at lower concentrations is lower. In all cases, the knee in the relation occurs at $0.5\lesssim N/N_{\text{theory}}\lesssim 0.8$. The knee is at a lower number for low angular velocities (open symbols) than for high angular velocities (black symbols) suggesting that higher inertia beads are more likely to retain large velocity fluctuations at higher number densities. The above remarks are intended to generate interest in this issue. Clearly, more

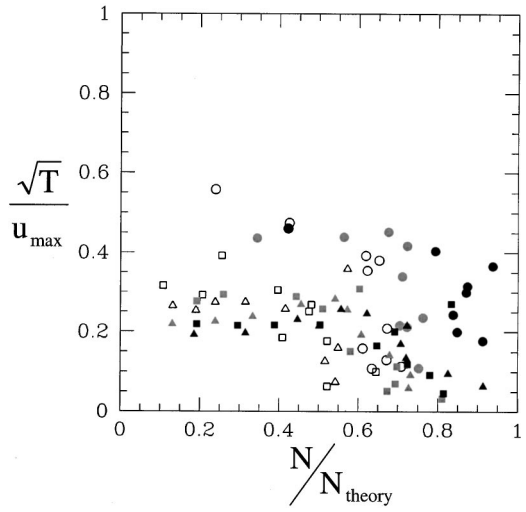

FIG. 13. Relation between velocity fluctuations and number density at $x=0$. Symbols: ▲, 1 mm beads; ■, 2 mm beads; ●, 3 mm beads. Symbol fill: open, 0.052 rad/s; gray, 0.094 rad/s; black, 0.168 rad/s.

research is necessary to clarify the relation between the temperature and the particle number density, perhaps accounting for the effect of overburden.

IV. CONCLUSIONS

Knowledge of flow dynamics of granular materials in a 2D rotating tumbler is key to the understanding of mixing and segregation of granular materials. For example, for polydisperse granular materials with beads differing in size, the flowing layer is responsible for segregation due to free surface segregation and particle percolation. Furthermore, a knowledge of the flow dynamics and scaling in 2D systems leads to further understanding of 3D granular systems and makes possible scale-up to larger systems.

Our results reveal a few key aspects of the flowing granular layer. Near the top of the flowing layer the streamwise velocity profile is nearly linear as shown in Fig. 6(b), while close to the interface between the layer and fixed bed the velocity logarithmically decreases to zero according to Fig. 7(a). Scaling based on the mass balance does not collapse the data for different bead sizes and angular velocities. However, normalizing with the maximum velocity at the top of the flowing layer shows a clear trend in the velocity profile.

The magnitude of the velocity fluctuations decrease with depth in the flowing layer. Near the surface of the flowing layer, the fluctuations can be as large as one-third the maximum streamwise velocity. The fluctuations decrease to less than one tenth of the free stream velocity near the fixed bed. However, near the fixed bed the velocity fluctuations are the same order as the local velocity. When the velocity fluctuations are normalized with the local streamwise velocity, the curves tend toward collapse and suggest an exponential dependence on the transverse coordinate.

Scaling the bead number profiles with a theoretical number density based on geometric arguments results in reasonable collapse of the number density profiles for different bead sizes and angular velocities. The number density changes appreciably in the upper half of the flowing layer, corresponding to the region in which the velocity profile is linear. However, the number density remains nearly constant in the lower half of the flowing layer, where the velocity profile is logarithmic. There also appears to be a weak trend relating the velocity fluctuations and the number density that is consistent with intuition.

ACKNOWLEDGMENTS

This work was funded by the Office of Basic Energy Sciences of the Department of Energy. We are grateful for the assistance of Dr. Alp Akonur in performing the experiments. We thank Professor Edwin A. Cowen of Cornell University for providing the particle tracking velocimetry code.

[1] H. Henein, J. K. Brimacomble, and A. P. Watkinson, "Experimental study of transverse bed motion in rotary kilns," Metall. Trans. B **14**, 191 (1983).
[2] J. Rajchenbach, "Flow in powders: From discrete avalanches to continuous regime," Phys. Rev. Lett. **65**, 2221 (1990).
[3] J. M. Ottino and D. V. Khakhar, "Mixing and segregation of granular materials," Annu. Rev. Fluid Mech. **32**, 55 (2000).
[4] T. S. Komatsu, S. Inagaki, N. Nakagawa, and S. Nasuno, "Creep motion in a granular pile exhibiting steady surface flow," Phys. Rev. Lett. **86**, 1757 (2001).
[5] J. M. Ottino, *The Kinematics of Mixing: Stretching, Chaos, and Transport* (Cambridge University Press, Cambridge, 1990).
[6] D. V. Khakhar, J. J. McCarthy, T. Shinbrot, and J. M. Ottino, "Transverse flow and mixing of granular materials in a rotating cylinder," Phys. Fluids **9**, 31 (1997).
[7] D. V. Khakhar, J. M. McCarthy, and J. M. Ottino, "Radial segregation of granular mixtures in rotating cylinders," Phys. Fluids **9**, 3600 (1997).
[8] M. Nakagawa, S. A. Altobelli, A. Caprihan, E. Fukushima, and E.-K. Jeong, "Non-invasive measurements of granular flows by magnetic resonance imaging," Exp. Fluids **16**, 54 (1993).
[9] G. H. Ristow, "Dynamics of granular materials in a rotating drum," Europhys. Lett. **34**, 263 (1996).
[10] B. F. C. Laurent, J. Bridgwater, and D. J. Parker, "Motion in a particle bed agitated by a single blade," AIChE J. **46**, 1723 (2000).
[11] G. W. Baxter, B. P. Behringer, T. Faggert, and G. A. Johnson, "Pattern formation in flowing sand," Phys. Rev. Lett. **62**, 2825 (1989).
[12] C. F. Harwood, "Powder segregation due to vibration," Powder Technol. **16**, 51 (1977).
[13] N. Menon and D. J. Durian, "Particle motions in a gas-fluidized bed of sand," Phys. Rev. Lett. **79**, 3407 (1997).
[14] A. A. Boateng and P. V. Barr, "Granular flow behavior in the transverse plane of a partially filled rotating cylinder," J. Fluid Mech. **330**, 233 (1997).
[15] H. Takahashi, A. Suzuki, and T. Tanaka, "Behavior of a particle bed in the field of vibration. I. Analysis of particle motion in a vibrating vessel," Powder Technol. **2**, 65 (1968–1969).
[16] S. Warr, G. T. H. Jacques, and J. M. Huntley, "Tracking the translational and rotational motion of granular particles: Use of high-speed photography and image processing," Powder Technol. **81**, 41 (1994).
[17] A. Medina, J. A. Cordova, E. Luna, and C. Trevino, "Velocity field measurements in granular flow in a near 2D silo," Phys. Lett. A **250**, 111 (1998).
[18] R. M. Lueptow, A. Akonur, and T. Shinbrot, "PIV for granular flows," Exp. Fluids **28**, 183 (1999).
[19] M. Tischer, M. I. Bursik, and E. B. Pitman, "Kinematics of sand avalanches using particle-image velocimetry," J. Sediment Res. **71**, 355 (2001).
[20] D. V. Khakhar, A. V. Orpe, P. Andresen, and J. M. Ottino, "Surface flow of granular materials: Model and experiments in heap formation," J. Fluid Mech. **441**, 255 (2001).
[21] E. Clément, J. Rajchenbach, and J. Duran, "Mixing of a granular material in a bidmensional rotating drum," Europhys. Lett. **30**, 7 (1995).
[22] G. Metcalfe, T. Shinbrot, J. J. McCarthy, and J. M. Ottino, "Avalanche mixing of granular solids," Nature (London) **374**, 39 (1995).

[23]J. Baxter, U. Tüzün, D. Heyes, I. Hayati, and P. Fredlund, ''Stratification in poured granular heaps,'' Nature (London) **391**, 136 (1998).
[24]A. Samandani, A. Pradhan, and A. Kudrolli, ''Size segregation in granular matter in silo discharges,'' Phys. Rev. E **60**, 7203 (1999).
[25]S. S. Hsiau and C. H. Chen, ''Granular convection cells in a vertical shaker,'' Powder Technol. **111**, 210 (2000).
[26]K. M. Hill, N. Jain, and J. M. Ottino, ''New modes of granular segregation in rotating cylinders,'' Phys. Rev. E **64**, 011302 (2001).
[27]J. M. Ottino and D. V. Khakhar, ''Fundamental research in heaping, mixing, and segregation of granular materials: Challenges and perspectives,'' Powder Technol. **121**, 117 (2001).
[28]E. A. Cowen and S. G. Monsmith, ''A hybrid digital particle tracking velocimetry technique,'' Exp. Fluids **22**, 199 (1997).
[29]A. V. Orpe and D. V. Khakhar, ''Scaling relations for granular flow in quasi-2d rotating cylinders,'' Phys. Rev. E **64**, 031302 (2001).
[30]C. S. Campbell, ''Rapid granular flows,'' Annu. Rev. Fluid Mech. **22**, 57 (1990).
[31]H. J. Hermann, ''On the thermodynamics of granular media,'' J. Phys. II **3**, 427 (1993).
[32]A. Caprihan and J. D. Seymour, ''Correlation time and diffusion coefficient imaging: Application to a granular flow system,'' J. Magn. Reson. **144**, 96 (2000).